Science of the Total Environment 654 (2019) 801–810

Contents lists available at ScienceDirect

Science of the Total Environment

journal homepage: www.elsevier.com/locate/scitotenv

# Increase in anthropogenic mercury in marginal sea sediments of the Northwest Pacific Ocean

Haryun Kim [a,1], Kitack Lee [a,*,2], Dhong-Il Lim [b,e,**,2], Seung-Il Nam [c], Seung hee Han [d], Jihun Kim [b,e], Eunil Lee [f], In-Seong Han [g], Young Keun Jin [c], Yanxu Zhang [h]

[a] Division of Environmental Science and Engineering, Pohang University of Science and Technology, Pohang, 37673, Republic of Korea
[b] South Sea Research Institute, Korea Institute of Ocean Science and Technology, Geoje 53201, Republic of Korea
[c] Korea Polar Research Institute, Incheon 21990, Republic of Korea
[d] School of Earth Sciences and Environmental Engineering, Gwangju Institute of Science and Technology (GIST), Gwangju 61005, Republic of Korea
[e] Department of Marine Environmental Science, University of Science and Technology, Daejeon 34113, Republic of Korea
[f] Ocean Research Division, Korea Hydrographic and Oceanographic Agency, Busan 49111, Republic of Korea
[g] Ocean Climate and Ecology Research Division, National Institute of Fisheries Science, Busan 46083, Republic of Korea
[h] School of Atmospheric Science, Nanjing University, Nanjing 210023, China

## HIGHLIGHTS

- The flux of $Hg^{ANTH}$ into sediments increased from the western Arctic Ocean to the East China Sea.
- The highest rate of $Hg^{ANTH}$ flux into sediments was found in the East China Sea.
- $Hg^{ANTH}$ has reached open ocean sediments over extended areas of the northwestern Pacific Ocean.

## GRAPHICAL ABSTRACT

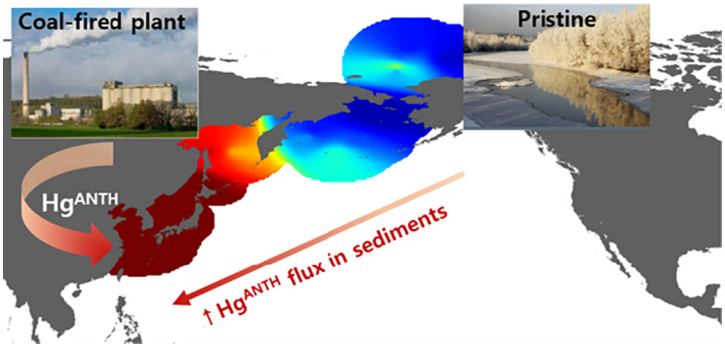


## ARTICLE INFO

*Article history:*
Received 11 July 2018
Received in revised form 5 November 2018
Accepted 6 November 2018
Available online 07 November 2018

Editor: Mae Sexauer Gustin

*Keywords:*
Total mercury
Anthropogenic Hg
Ocean sediment

## ABSTRACT

Over the past century, the addition of anthropogenic mercury ($Hg^{ANTH}$) to vast areas of North Pacific marginal seas adjacent to the northeast Asian continent has tripled. Analysis of sediment cores showed that the rate of $Hg^{ANTH}$ addition ($Hg^{ANTH}$ flux) was greatest in the East China and Yellow Seas (9.1 μg $m^{-2}$ $yr^{-1}$) in the vicinity of China (the source continent), but was small in the Bering and western Arctic Ocean (Chukchi Sea) (0.9 μg $m^{-2}$ $yr^{-1}$; the regions furthest from China). Our results show that $Hg^{ANTH}$ has reached open ocean sedimentary environments over extended areas of the northwestern Pacific Ocean, via the formation of organic-mercury complexes and deposition. The implication of these findings is that the addition of $Hg^{ANTH}$ (via atmospheric deposition and riverine input) to the ocean environment is responsible for elevated Hg flux into sedimentary environments in the northwest Pacific Ocean.



* Correspondence to: K. Lee, Division of Environmental Science and Engineering, Pohang University of Science and Technology, Pohang, 37673, Republic of Korea.
** Correspondence to: D. Lim, South Sea Research Institute, Korea Institute of Ocean Science and Technology, Jangmok 53201, Republic of Korea.
*E-mail addresses:* ktl@postech.ac.kr (K. Lee), oceanlim@kiost.ac.kr (D.-I. Lim).
[1] Present address: Fundamental Research Division, National Marine Biodiversity Institute of Korea, Janghang, 33662, Republic of Korea.
[2] These authors contributed equally to this work.

https://doi.org/10.1016/j.scitotenv.2018.11.076
0048-9697/

## 1. Introduction

Gaseous elemental mercury ($Hg^0$) emitted from natural and anthropogenic sources is photochemically oxidized to reactive mercury ($Hg^{2+}$) in the atmosphere. If deposited onto the ocean surface (primarily via wet and dry deposition), some of the $Hg^{2+}$ can be reduced to $Hg^0$ in the surface waters and re-emitted to the atmosphere, and some is absorbed onto suspended particulate matter to produce particulate Hg ($Hg^P$), and then deposited into sediments. Other established pathways for $Hg^{2+}$ include conversions to insoluble mercury sulfide, which settles out of the water column and is incorporated into sediments or converted to the more toxic methylmercury ($CH_3Hg^+$) by methanogenic (methane producing) and sulfate-reducing bacteria in restricted anaerobic conditions. These toxic $CH_3Hg^+$ are released by anaerobic bacteria as a dissolved form, consumed by phytoplankton and zooplankton at higher tropic levels, and accumulated in the food chain, from where it can eventually be incorporated into sediments in the form of organo mercury complexes (Engstrom, 2007; Percival et al., 2015).

Mercury isotope compositions (e.g., $\Delta^{199}Hg$, $\Delta^{200}Hg$, $\delta^{202}Hg$) of various Hg sources are widely used as a basis for discriminating anthropogenic Hg ($Hg^{ANTH}$) from Hg derived from other natural emissions (Blum et al., 2014; Lepak et al., 2015). However, the isotope composition of sediment Hg can be complicated by either isotope fractionation (depending on the mass of the Hg isotopes, MDF) or isotope separation (in no proportion to the difference in the mass of the isotopes, MIF) in the atmosphere and the ocean, prior to its deposition into sediments (Blum et al., 2014; Sun et al., 2014; Enrico et al., 2017). Moreover, microbial-mediated reactions (e.g. methylation and demethylation), chemical reactions (e.g. photo-reduction or chemical reduction) and purely physical processes (e.g. volatilization, evaporation, adsorption, and dissolution) all yield additional MDF and MIF in aquatic environments, and thereby alter the isotope composition of sediment Hg. Moreover, the isotope values of anthropogenic sources of Hg overlap, which makes estimation of the contributions of various anthropogenic sources to sediment Hg ambiguous. As a result, studies using methods based on isotope composition data have been mostly performed in restricted basins having a few dominant sources (Sherman et al., 2012; Lepak et al., 2015; Wiederhold et al., 2015), and not in open ocean ecosystems having numerous sources (Yin et al., 2015).

Measurement of the Hg content in ice cores is a newly introduced method of estimating the $Hg^{ANTH}$ input to terrestrial or ocean ecosystems (Schuster et al., 2002). However, this method is only applicable to high latitudes including the Arctic region or temperate glaciers where ice cores record the input history of Hg. Therefore, another method is needed for the northwestern Pacific Ocean where $Hg^{ANTH}$ input was reported to be largest. The Hg accumulation rate (i.e. the Hg flux) in sediment is an alternative method of identifying $Hg^{ANTH}$ inputs if the physical and chemical effects (i.e. grain size, organic matter content, sedimentation rate and Fe/Mn reduction) on the Hg accumulation rate are properly taken into account, because these rates can reflect the historical trend of Hg accumulation and are consistent with atmospheric Hg deposition rate data.

The atmospheric deposition of $Hg^{ANTH}$ to the open ocean is estimated to be 5200–6600 Mg $yr^{-1}$ (Holmes et al., 2010; Corbitt et al., 2011) that is twice that of riverine input (Sunderland and Mason, 2007; Amos et al., 2014). Therefore, $Hg^{ANTH}$ could be discernable in offshore sedimentary environments. The majority of studies performed to date have focused on the total (anthropogenic plus natural) content of Hg in estuarine or coastal shelf sediments that are primarily influenced by riverine $Hg^{ANTH}$ (Covelli et al., 2001; Johannessen et al., 2005; Morris et al., 2014). Studies have not considered the influence of $Hg^{ANTH}$ on the open ocean sedimentary environments because data on sediment Hg content from widespread open ocean areas are limited, and more importantly, a reliable method to account for regional variations in the sediment Hg content is not yet available. Consequently, some studies on the influence of $Hg^{ANTH}$ on offshore sedimentary environments have taken an indirect approach, relying on modeled results derived from Hg emission data rather than field measurements (Sunderland and Mason, 2007; Amos et al., 2014).

A key hurdle in determining the content of $Hg^{ANTH}$ in a sedimentary environment is to estimate the natural level of Hg, and then to subtract this from the total Hg content. However, the accurate estimation of the natural level of Hg in sediment is not straightforward because the adsorption of Hg onto particles (which directly influences the Hg flux) in the water column immediately above the sediment being sampled is sensitive to the physical and chemical properties of those particles. Due to this inherent difficulty, the majority of studies have focused on limited areas having similar natural levels of Hg and similar water column particles associated with Hg (Covelli et al., 2001; Johannessen et al., 2005; Morris et al., 2014; Zhou et al., 2014; Zohar et al., 2014). These studies involved a simple comparison of the sedimentary Hg concentrations or total sedimentary Hg flux between pre-industrial and industrial periods, or in contaminated and less contaminated regions (Covelli et al., 2001; Johannessen et al., 2005; Morris et al., 2014; Zhou et al., 2014). Therefore, to better understand the occurrence of $Hg^{ANTH}$ in open ocean sedimentary environments, studies investigating extensive ocean regions from contaminated to less contaminated regions should be performed, and importantly the natural levels of Hg need to be accurately estimated.

In this context, we assessed the influence of $Hg^{ANTH}$ on the ocean sedimentary environments by analyzing the sedimentary Hg flux for 319 surface sediments and in several sediment cores obtained from all basins in our study area, including the East China and Yellow Seas, East Sea, Okhotsk Sea, Bering Sea, and the western Arctic Ocean (Chukchi Sea). We also assessed the % fraction of $Hg^{ANTH}$ accumulated in each sedimentary environment relative to the total $Hg^{ANTH}$ input (via atmospheric deposition and riverine inputs) into each basin.

## 2. Materials and methods

### 2.1. Study sites

The study sites were located over an area extending from the East China and Yellow Seas in the south to as far north as the western Arctic Ocean. The East China and Yellow Seas are close to the Chinese coast (the major $Hg^{ANTH}$ source), whereas the Bering Sea and the western Arctic Ocean are far from China and regarded as being more pristine. All of the basins examined here are located downwind of the major $Hg^{ANTH}$ source country (China) and thus, westerly winds carry gaseous elemental $Hg^0$ progressively less from the East China and Yellow Seas to the western Arctic Ocean, resulting in a northeastward decrease in $Hg^{ANTH}$ deposition. Each basin receives additional Hg via riverine flux: the Changjiang and Huang He rivers flow into the East China and Yellow Seas, respectively; and the Amur and Yukon rivers flow into the Okhotsk Sea and the western Arctic Ocean, respectively (Table 1). The basins examined here receive varying amounts of $Hg^{ANTH}$ via atmospheric deposition and riverine flux based on models. The East China and Yellow Seas have the highest $Hg^{ANTH}$ flux (approximately 133 μg $m^{-2}$ $yr^{-1}$ and 86 μg $m^{-2}$ $yr^{-1}$, respectively) (Sunderland and Mason, 2007; Corbitt et al., 2011; Percival et al., 2015), followed by the East Sea (approximately 33 μg $m^{-2}$ $yr^{-1}$) (Amos et al., 2014), the Okhotsk Sea (approximately 10 μg $m^{-2}$ $yr^{-1}$), the Bering Sea (approximately 8 μg $m^{-2}$ $yr^{-1}$), and the western Arctic Ocean (lowest and approximately 5 μg $Hg^{ANTH}$ $m^{-2}$ $yr^{-1}$) (Zhang et al., 2016).

### 2.2. Sediment sampling methods

Single surface sediment was sampled from each of 268 sites in the Huang He ($n = 22$) and Changjiang ($n = 24$) estuaries, and from the East China ($n = 27$) and Yellow ($n = 195$) Seas using a grab sampler or a box corer over various Korea Institute of Ocean Science and Technology expeditions conducted since 2000. One sediment core from the

**Table 1**
Characteristics of the basins from which sediment samples were taken, and the rivers flowing into each basin.

| Basin | Water depth (m) | Area ($km^2$) | River |
|---|---|---|---|
| East China Sea | <50 | 1,249,000 | Changjiang |
| Yellow Sea | <50 | 380,000 | Huang He |
| East Sea | 977 | 978,000 | |
| Okhotsk Sea | 1213 | 1,583,000 | Amur |
| Bering Sea | 1766 | 2,000,000 | |
| Western Arctic Ocean | 1062 | 620,000 | Yukon |

East China Sea and two sediment cores from the Yellow Sea were also collected using box and piston cores. Note that data on the Huang He and Changjiang estuaries and the East China and Yellow sea sediments were obtained from the literature (Lim et al., 2017; Kim et al., 2018).

The sediment cores collected using a multi/gravity corer were also taken from the East Sea ($n = 3$), the Okhotsk Sea ($n = 2$), and the western Arctic Ocean ($n = 2$); the latter were collected along with the western Arctic Ocean surface sediments ($n = 5$) during Korea Polar Research Institute expeditions conducted using RV Araon between 2010 and 2013. All sediment samples were stored onboard at −20 °C, samples were freeze-dried for 4 days, and then ground to a powder using a mortar and pestle.

We additionally included data on the concentrations of Hg, total organic carbon (TOC), and Al, and mass accumulation rates (MAR) for 39 sites in the East ($n = 3$), Okhotsk ($n = 25$), and Bering ($n = 11$) Seas; these data were obtained from literatures. Detail information on the sampling methods and sites is summarized in Table 2, and Tables S1, S2 and S3 in the Supplementary Information.

### 2.3. Concentrations of total Hg, Al, Fe and TOC in sediments

Total Hg (THg) concentrations were measured using an automatic Hg analyzer, and involved thermal decomposition followed by catalytic reduction, amalgamation, desorption, and the use of an atomic absorption module (model Hydra II Direct Hg analyzer; Teledyne Leeman Labs, Hudson, NH, USA), and were calibrated against marine sediment reference materials (MESS-3; Hg = 91 ± 9 ng $g^{-1}$ certified by the National Research Council of Canada) for trace metals and other constituents. The analytical accuracies were determined to be <5%, based on replicate analysis of the certified reference materials (MESS-3), and the analytical precision in measurements of the THg concentration was determined to be <10%, based on replicate measurements of standard materials and sediment samples. For determining the concentrations of Al and Fe, the powered samples including a standard reference material (MAG-1; $Al_2O_3 = 16.4 \pm 0.3\%$ and $Fe_2O_3 = 6.8 \pm 0.6\%$; certified by U.S. Geological Survey) were dissolved in a mixture of hydrofluoric and perchloric acids, and the elemental concentrations were measured using inductively coupled plasma atomic emission spectroscopy (Spectro Flame Modula EOP; SPECTRO Analytical Instruments Inc., Kleve, Germany). The analytical accuracy and precision ranged from 5% to 10%, and the concentrations were then calibrated against Marine Sediment-1 reference material (certified by the U.S. Geological Survey) (Lim et al., 2012). The concentrations of total carbon (TC), and total inorganic carbon (TIC) in the dried and ground sediment samples were measured using a Thermo Electron Corporation Flash EA 1112 Series NC Soil Analyzer for TC, and a $CO_2$ coulometer (model CM5014; UIC Inc.) for TIC (Waltham, MA, USA). The accuracy and precision in analysis of these elements were <5%, based on analysis of standard reference materials ($_L$-cysteine in the TC analysis, and calcium carbonate having 12% C in the TIC analysis). TOC concentrations were calculated by subtracting TIC from TC (Nelson, 1996). Note all data that we used in our analysis are presented in Table S3 in the Supplementary Information.

### 2.4. Sedimentation rate for sediment cores

The sedimentation rates for 7 sediment cores (Yellow Sea I, II; East Sea I, II, III; Okhotsk Basin; western Arctic Ocean) were measured using excess $^{210}Pb$ ($^{210}Pb_{ex}$) activity, which is equivalent to the total $^{210}Pb$ activity ($^{210}Pb_{tot}$) minus the $^{210}Pb$ activity supported by an indigenous parent radionuclide (Lim et al., 2007; Lim et al., 2012). All sediment cores were sectioned at intervals of 2–5 cm, and were then freeze-dried and powdered. For age analysis, 5 g of the powdered sediment was added to acidic solution and spiked with $^{209}Po$ for leaching. After drying the $^{209}Po$ was dissolved in 1 M HCl and separated from the acidic solution using a centrifuge. The $^{209}Po$ in particles was then plated onto a silver planchet, and $^{210}Pb$ activities were determined by counting the alpha decay of its grand-daughter isotope $^{210}Po$ (Lim et al., 2007). The sedimentation rate for the East China Sea core was calculated on the basis of the accelerator mass spectrometry (AMS) $^{14}C$ age (1030 ± 40 year before present) of foraminifera at a core depth of 150 cm (Dou et al., 2015). The ages of cores from the Okhotsk Basin were obtained from published scientific reports (Table 2) (Astakhov et al., 2005; Chen et al., 2016). Mass accumulation rates (= sedimentation rate × dry bulk density) for all basins were obtained from the literatures and summarized in Table 2.

**Table 2**
Information on the surface sediments used in this study.

| Basins | No. | Hg | MAR | $Hg^{ANTH}$ flux | Age | Texture | Al | TOC | Reference |
|---|---|---|---|---|---|---|---|---|---|
| | | (ng $g^{-1}$) | (g $cm^{-2}$ $yr^{-1}$) | (μg $m^{-2}$ $yr^{-1}$) | (y) | | (%) | (mg $g^{-1}$) | |
| Huang He River | 22 | 20 ± 3 | 0.5 | 38 ± 14 | – | – | 6 ± 0.1 | 3 ± 0.4 | Kim et al., 2017; Lim et al., 2017; Kim et al., 2018; Hu et al., 2016 |
| Changjiang River | 24 | 105 ± 11 | 0.87 | 776 ± 56 | – | – | 7.4 ± 0.1 | 7 ± 0.5 | Lim et al., 2017; Kim et al., 2018; Deng et al., 2006; Fang et al., 2009 |
| East China Sea | 27 | 18 ± 1 | 0.2 | 9 ± 2 | 8 ± 10 | calcareous ooze, sand | 6.4 ± 0.2 | 5 ± 0.4 | Lim et al., 2017; Kim et al., 2018; Dou et al., 2015 |
| Yellow Sea | 195 | 19 ± 1 | 0.15 | 8 ± 1 | 8 ± 2 | siliceous mud | 6.5 ± 0.1 | 5 ± 0.2 | Lim et al., 2017; Kim et al., 2018 |
| East Sea | 8 | 89 ± 22 | 0.02 | 11 ± 4 | 18 ± 10 | clay, siliceous mud | 5.3 ± 0.8 | 18 ± 5 | Song et al., 2015; Hong et al., 1997 |
| Okhotsk Sea | 27 | 91 ± 30 | 0.02 | 5 ± 1 | 42 ± 15 | clay, siliceous mud, diatom ooze | 4.6 ± 0.2 | 15 ± 1.2 | Astakhov et al., 2005 |
| Bering Sea | 11 | 45 ± 9 | 0.07 | 0.4 ± 0.3 | 20 | clay, diatom ooze, sandy silt, siliceous mud | 3.9 ± 0 | 9 ± 0.9 | Iricanin and Trefry, 1990; Oguri et al., 2012 |
| Western Arctic Ocean | 7 | 78 ± 8 | 0.04 | 0.9 ± 0.7 | 8 ± 4 | siliceous mud, silt, slay, sand | 7.0 ± 0.2 | 12 ± 1.5 | Chen et al., 2016 |

### 2.5. Calculation of $Hg^{ANTH}$ flux

The absolute concentration of Hg in sediment is primarily determined by the rate of sedimentation, and to a lesser but significant extent by the physical properties of the sediment, including sediment texture (grain size), organic matter content, porosity and compaction (Daskalakis and O'Connor, 1995). Our measurements showed that the Hg concentrations in sediment samples from the western Arctic Ocean are generally higher than in those from the East China and Yellow Seas (Table 2 and Table S3, Fig. S1 in the Supplementary Information). Therefore, if the absolute concentration of Hg were to be used to estimate $Hg^{ANTH}$ input into sedimentary environments, the Arctic sedimentary environment would be determined to receive more Hg than the East China and Yellow Seas. However, to compare $Hg^{ANTH}$ inputs into the various sedimentary environments of our study area, we must first account for basin-to-basin differences in sediment Hg content associated with differences in sedimentation rate and the physical properties of the sediments. Therefore, instead of using the absolute Hg concentration (ng $g^{-1}$) in sediment samples, we use the total Hg flux (μg $m^{-2}$ $yr^{-1}$) into the sediments (Fig. S2 in Supplementary Information) calculated using the equation:

$$\text{Total Hg flux } (\mu g\ m^{-2}\ yr^{-1}) = (\text{sedimentation rate x } \rho_{SED})\ \text{x } [Hg]_{SED} \quad (1)$$

where MAR (g $cm^{-2}$ $yr^{-1}$) is the mass accumulation rate that is the product of the sedimentation rate (cm $yr^{-1}$) and dry bulk density ($\rho_{SED}$ g $cm^{-3}$); and $[Hg]_{SED}$ (Fig. S1 in the Supplementary Information) is the total sediment concentration of Hg (ng $g^{-1}$). Here, MAR was calculated using the dry bulk density in order to remove the difference in total Hg content arising from differences in the physical properties of sediments (e.g. sediment texture and porosity).

Next, we must separate the $Hg^{ANTH}$ flux (Fig. 3B) from the total Hg flux (Fig. S2 in the Supplementary Information; anthropogenic and natural components combined). To achieve this, we used the sediment Hg to Al concentration ratio measured in the sediment core samples. This method of normalization, which has been found to be robust, commonly uses the sediment Al content because Al is the most abundant component of aluminosilicate minerals and clays, and derives only from natural sources (no anthropogenic source exists) (Loring and Rantala, 1992). Moreover, compared to sands and silts, clay minerals tend to have the larger surface areas, and thereby facilitating direct contact with greater numbers of Hg atoms. The strong link between Hg and clays is supported by the observation of positive correlations between Al, clay, and Hg contents (Loring and Rantala, 1992). Thus, given that Al comes almost exclusively from natural sources (predominantly from the weathering of bedrocks in watersheds), the natural Hg fraction can be determined by normalization of the sediment Hg content by sediment Al content.

Normalization of the Hg content by the Al content in sediment samples is therefore a useful method for accounting for temporal and regional variations in Hg content associated with variations in sediment texture (grain size) and bedrock weathering. The Hg content in sediment samples is expressed as the enrichment factor of Hg ($EF_{Hg}$) that was calculated by dividing the Hg/Al ratio for surface or core samples ($[Hg/Al]_{SAMP}$) by the same ratio for $Hg^{ANTH}$-free samples ($[Hg/Al]_{BACKGROUND}$) collected during the pre-industrial era:

$$EF_{Hg} = [Hg/Al]_{SAMP}/[Hg/Al]_{BACKGROUND} \quad (2)$$

The accuracy of this normalization depends on the consistency in $Hg/Al_{BACKGROUND}$ within each basin. For all basins examined, we found no significant differences in the background Hg/Al ratios obtained from $Hg^{ANTH}$-free sediment core samples within each basin. This indicates that a unique $Hg/Al_{BACKGROUND}$ ratio was identified for each basin that could then be used to normalize the total $(Hg/Al)_{SAMP}$ ratios measured throughout sediment cores and for all surface sediment samples in such a way to calculate $EF_{Hg}$ and hence the flux of $Hg^{ANTH}$ (Fig. 1).

Finally, the $Hg^{ANTH}$ flux to sediments is calculated using Eq. (3) by subtracting the background flux for Hg: $\{([Hg] \times MAR)_{SAMP}/EF_{Hg}\}$ (Fig. S3 in the Supplementary Information) from the total flux for Hg: $([Hg] \times MAR)_{SAMP}$ (Fig. S2 in the Supplementary Information) (Hermanns and Biester, 2013):

$$Hg^{ANTH}\text{flux } (\mu g\ m^{-2}\ yr^{-1}) = ([Hg] \times MAR)_{SAMP} - \{([Hg] \times MAR)_{TOTAL}/EF_{Hg}\} \quad (3)$$

Variations in the organic matter content of sediments also influence the concentration of Hg, because Hg has a strong affinity for organic matter (Chakraborty et al., 2015). The strong positive correlations we observed between the sediment Hg/Al and Hg/TOC ratios for all basins examined (Fig. 2) indicate that the Al-based normalization can satisfactorily account for variations in sediment Hg associated with sediment grain size and organic matter content. Therefore, additional correction for variations in the concentration of organic matter was not needed.

### 2.6. Statistical methods

The distribution of $Hg^{ANTH}$ flux in Fig. 3A was created using Ocean data view (Version 5.1) and the other plots (Figs. 1, 2, 3B, 4 and 5) were created using a sigma plot (Version 13.0). The statistical analysis between chemical parameters and Hg contents were performed using a R soft program.

## 3. Results

### 3.1. Geochemical properties of surface sediments

The concentration of Hg in sediment was found to be the highest in the Changjiang River estuary, followed by the Okhotsk Sea, the East Sea, the western Arctic Ocean, the Bering Sea, and the Yellow and East China Seas (Table 2). As the absolute concentration of sediment Hg is closely associated with MAR, the Changjiang River basin had the highest MAR (0.87 g $cm^{-2}$ $yr^{-1}$) and then MAR progressively decreased in accordance with the order of sediment Hg content. With the exception of sediments obtained from the Okhotsk Sea and deep western Arctic Ocean, surface sediments from all basins were deposited within the last 17 y, indicating that most surface sediments used in our analysis would likely to have contained discernable amounts of $Hg^{ANTH}$ (Table 2).

In terms of sediment texture, sediments from the East China and Yellow Seas consist largely of sand and mud, respectively, whereas the East Sea and the western Arctic Ocean sediments consist of clays and are rich in organic carbon. The Okhotsk and Bering sea sediments consist largely of a mixture of clay, silt and sand (Müller et al., 2016).

Sediment Al content is higher in the western Arctic Ocean than in other basins, whereas TOC content is higher in the East, Okhotsk Seas and western Arctic Ocean. The East China and Yellow Seas are shallow basins (100 m depth), whereas the East, Okhotsk, and Bering Seas are more like deep basins (977 m for the East Sea to 1766 m for the Bering Sea). The physical properties of samples from the various seas are more summarized in Table 2 and in Supplementary Information Tables S1 and S2.

### 3.2. The background ratio of Al concentration to Hg concentration in sediment

For each basin in our study area, the background ratio of the Hg concentration to the Al concentration (the ratio representing sediment accumulated during the pre-industrial era before 1900) was derived from two or three sediment cores. The differences in the resulting background Hg/Al ratio were not statistically significant within individual

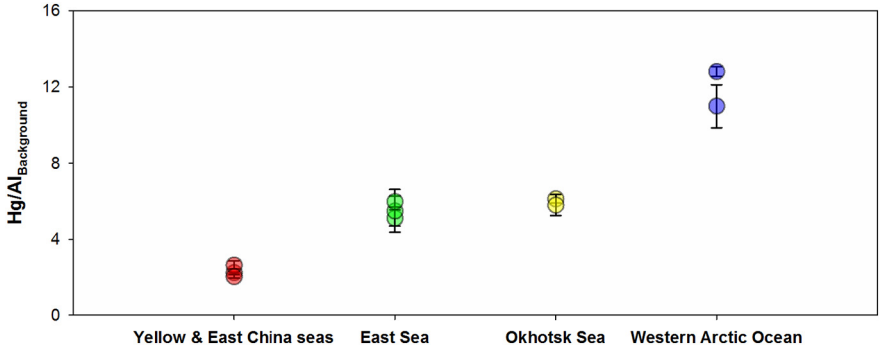


**Fig. 1.** The ratios of Hg to Al for the background sediment samples. The samples were obtained from cores of sediment that accumulated during the pre-industrial times in the Yellow ($n = 2$; red) and East China ($n = 1$; red) seas, the East Sea ($n = 3$; green), the Okhotsk Sea ($n = 2$; yellow) and the western Arctic Ocean ($n = 2$; purple). (For interpretation of the references to color in this figure legend, the reader is referred to the web version of this article.)

basins, and this background ratio increased in a northeastward direction from the Yellow and East China Seas to the western Arctic Ocean (Fig. 1).

### 3.3. Spatial distribution of $Hg^{ANTH}$ flux in sediments of the Northwest Pacific Ocean

The highest rate of $Hg^{ANTH}$ addition was found in sediments in close proximity to the Changjiang ($776 \pm 56$ μg $m^{-2}$ $yr^{-1}$; $n = 24$) and Huang He ($38 \pm 14$ μg $m^{-2}$ $yr^{-1}$; $n = 22$) river estuaries. For remote open ocean sedimentary environments (except for the East China and Yellow Seas where riverine input of Hg is equally important), which mainly receive $Hg^{ANTH}$ by atmospheric deposition, higher rates of $Hg^{ANTH}$ were found in the East China ($9 \pm 2$ μg $m^{-2}$ $yr^{-1}$; $n = 27$), Yellow ($8 \pm 0.8$ μg $m^{-2}$ $yr^{-1}$; $n = 195$) and East ($11 \pm 4$ μg $m^{-2}$ $yr^{-1}$; $n = 6$) Seas than were found in the Okhotsk ($5 \pm 1$ μg $m^{-2}$ $yr^{-2}$; $n = 27$) and Bering ($0.4 \pm 0.3$ μg $m^{-2}$ $yr^{-1}$; $n = 11$) Seas, and the western Arctic Ocean ($0.9 \pm 0.7$ μg $m^{-2}$ $yr^{-1}$, $n = 7$) (Table 2). These locations are increasingly distant from the major source continent for $Hg^{ANTH}$ (Fig. 3A).

### 3.4. Down-core variations in sedimentary $Hg^{ANTH}$ flux in the Northwest Pacific Ocean

The historical trends of $Hg^{ANTH}$ input to the northwestern Pacific Ocean marginal sea sediments were obtained from analysis of core sediments sampled from all basins. During the industrial era (~1900s onwards for Asian countries), the $Hg^{ANTH}$ flux increased in all basins except the western Arctic Ocean (Fig. 3B). $Hg^{ANTH}$ flux was generally

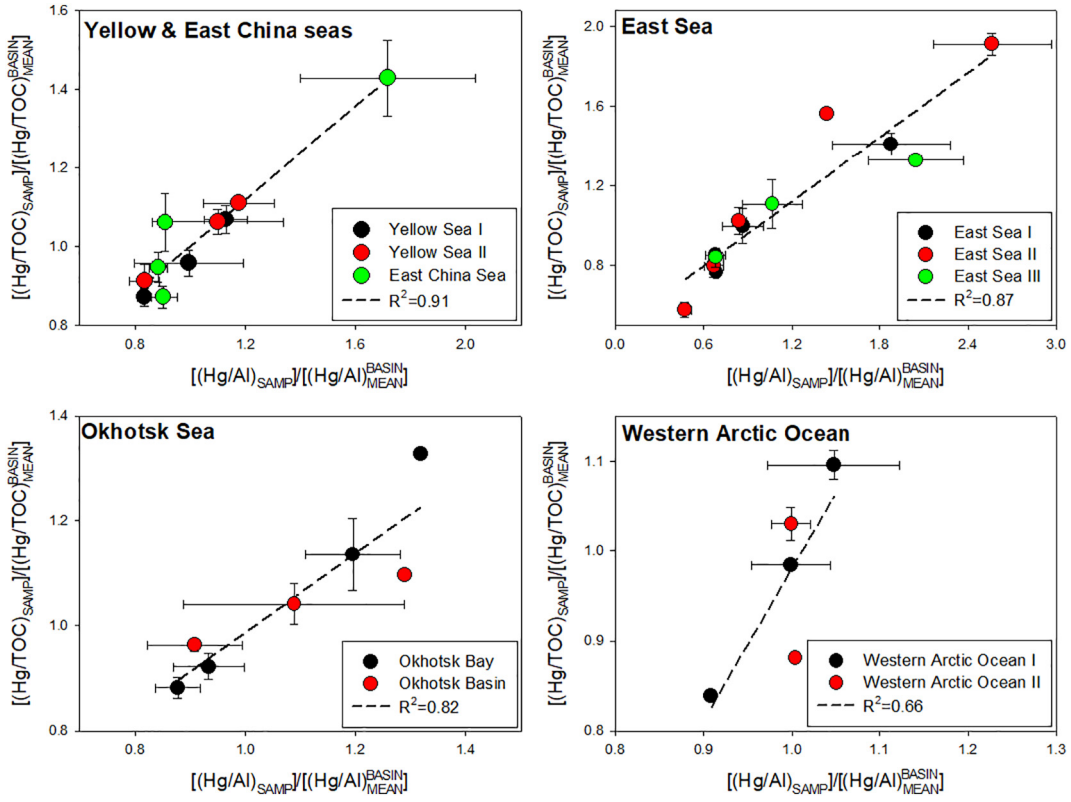


**Fig. 2.** The relationships between Hg/TOC ratios and Hg/Al ratios in the sediment depth profiles from the Yellow, East China, East, and Okhotsk Seas, and the western Arctic Ocean. As the effect of $Hg^{ANTH}$ input on sediment Hg/Al or Hg/TOC ratios differed among the basins, we sought to minimize the effect of such basin-to-basin difference by normalizing each sediment sample value ($[Hg/Al]_{SAMP}$) to the corresponding basin-mean background values ($[Hg/Al]_{MEAN}^{BASIN}$ or $[Hg/TOC]_{MEAN}^{BASIN}$). Samples from the western Arctic Ocean II did not show the positive relationship because all data except one were clustered in terms of the Hg/Al ratio. (For interpretation of the references to color in this figure legend, the reader is referred to the web version of this article.)

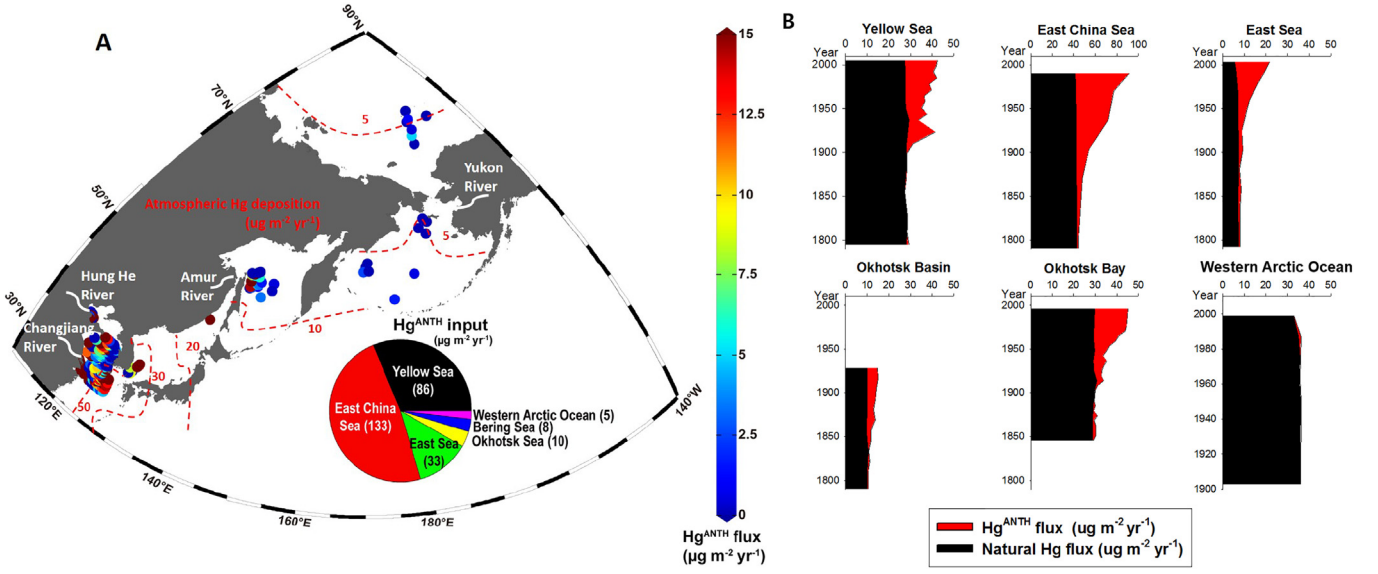


**Fig. 3.** Spatial and historical distributions of $Hg^{ANTH}$ flux in the northwestern Pacific Ocean sediments. (A) $Hg^{ANTH}$ flux deposited to surface sediments (Circles) in the Huang He ($n = 22$) and Changjiang ($n = 24$) estuaries, and the East China Sea ($n = 27$), the Yellow Sea ($n = 195$), the East Sea ($n = 6$), the Okhotsk Sea ($n = 27$), the Bering Sea ($n = 11$), and the western Arctic Ocean ($n = 7$). The dash line indicates the atmospheric Hg deposition and the pie graph is the input of riverine and atmospheric $Hg^{ANTH}$ to the East China and Yellow Seas and the input of atmospheric $Hg^{ANTH}$ to the East, Okhotsk, and Bering Seas and the western Arctic Ocean (Amos et al., 2014; Liu et al., 2016; Zhang et al., 2015, 2016). (B) The $Hg^{ANTH}$ flux in the cores from the East China Sea, the Yellow Sea, the East Sea, Okhotsk Bay and Basin, and the western Arctic Ocean (Horizontal bar chart; black: Natural Hg flux; red: $Hg^{ANTH}$ flux). (For interpretation of the references to color in this figure legend, the reader is referred to the web version of this article.)

higher in the sediments of the East China and Yellow Seas, and sharply decreased in a northeastward direction toward the Okhotsk Sea and western Arctic Ocean. It is notable that the Hg flux (largely natural plus minor anthropogenic) to the western Arctic Ocean sediments remained unchanged during the pre-industrial and industrial eras (Fig. 3B).

### 3.5. Hg contents relative to other elements (TOC, Al, and Fe) in core sediments

To investigate the effects of all possible processes (i.e. grain size, organic matter content, redox cycling and change of sedimentation rates) on the historical trend in Hg contents in the sediment core samples, the sediment Hg content was plotted against the Hg/Al and Hg/TOC ratios for all sediment cores collected from the same basin. For each basin, the sediment Hg content was strongly related to the Hg/Al or Hg/TOC ratios (Fig. 4), and not related to the sediment Fe contents (Fig. 5 and Fig. S4 in Supplementary Information). Note that we did not find discernable change in sedimentation rate for all sediment cores (Fig. S5 in Supplementary Information).

## 4. Discussion

### 4.1. Properties of surface sediments in the Northwest Pacific Ocean

The basin-to-basin variations in natural Hg concentration were mainly attributed to the bedrock type in the watershed of the basins, where weathering leaches out the Hg, Al, and other minerals and subsequently delivers them to the basins. For example, the background Hg concentration was reported to be 22 ng $g^{-1}$ (Chen et al., 2013; Huang et al., 2005) for Lake Tai in the vicinity of the Changjiang River (China), and 100 ng $g^{-1}$ (Fitzgerald et al., 2005) for the northern Alaska. These background Hg concentrations are consistent with the pre-industrial (since 1900) values for several sediment cores obtained from the East China and Yellow Seas and the western Arctic Ocean, respectively (Fig. S1 in the Supplementary Information). Moreover, the higher Al content in the western Arctic Ocean sediment indicates that the sediments in that ocean probably receive higher levels of natural Hg by weathering of bedrocks (Table 2). Consequently, the higher natural Hg content in the western Arctic Ocean relative to the East China Sea was probably because of differences in indigenous Hg levels rather than anthropogenic influences.

A key requirement in our calculation of the flux of $Hg^{ANTH}$ into surface sediments is that the ages of the top-core sediments sampled across the study area are similar, because surface sediments with extremely low sedimentation rates may contain natural Hg deposited prior to the industrial period. According to this criterion, we excluded from our analysis some open western Arctic basin samples (close to 1000 years old) but included the western Arctic shelf samples. Most surface sediment samples used in this study are similar in age (17 ± 12 y), indicating that they contained an anthropogenic Hg component that accumulated during the industrial period (Table 2).

### 4.2. Distribution of surface sediment $Hg^{ANTH}$ flux in the Northwest Pacific Ocean

The flux of $Hg^{ANTH}$ in all basins of our study area is generally consistent with the northeast decrease in the input of $Hg^{ANTH}$ from the Yellow and East China Seas (<133 μg $m^{-2}$ $yr^{-1}$) (Liu et al., 2016) to the western Arctic Ocean (5 μg $m^{-2}$ $yr^{-1}$) (Amos et al., 2014) (Fig. 3A). This indicates that the addition of $Hg^{ANTH}$ leads to an increase in the burial of $Hg^{ANTH}$ in open ocean sediments. Based on the rates of input of $Hg^{ANTH}$ and its subsequent accumulation in sediments, it was estimated that approximately 8% of the deposited $Hg^{ANTH}$ accumulates in sediments of the Yellow and East China Seas, which is broadly consistent with the global average value of 5%. This finding implies that the open ocean sediments act as a sink for $Hg^{ANTH}$.

The recent increase in $Hg^{ANTH}$ addition to the East China Sea and Okhotsk Bay indicates that the $Hg^{ANTH}$ from the Changjiang (581 ± 541 Mg $yr^{-1}$) (Zhang et al., 2015) and Amur (68 ± 52 Mg $yr^{-1}$) (Zhang et al., 2015) rivers has spread by ocean currents into extensive areas of the East China Sea and Okhotsk Bay, respectively (Liu et al., 2016) (Fig. 3). However, the absence of a discernable change in the sedimentary input of Hg to the western Arctic Ocean during the past 200 years indicates that little $Hg^{ANTH}$ has reached the western Arctic Ocean by atmospheric transport and deposition. This is consistent

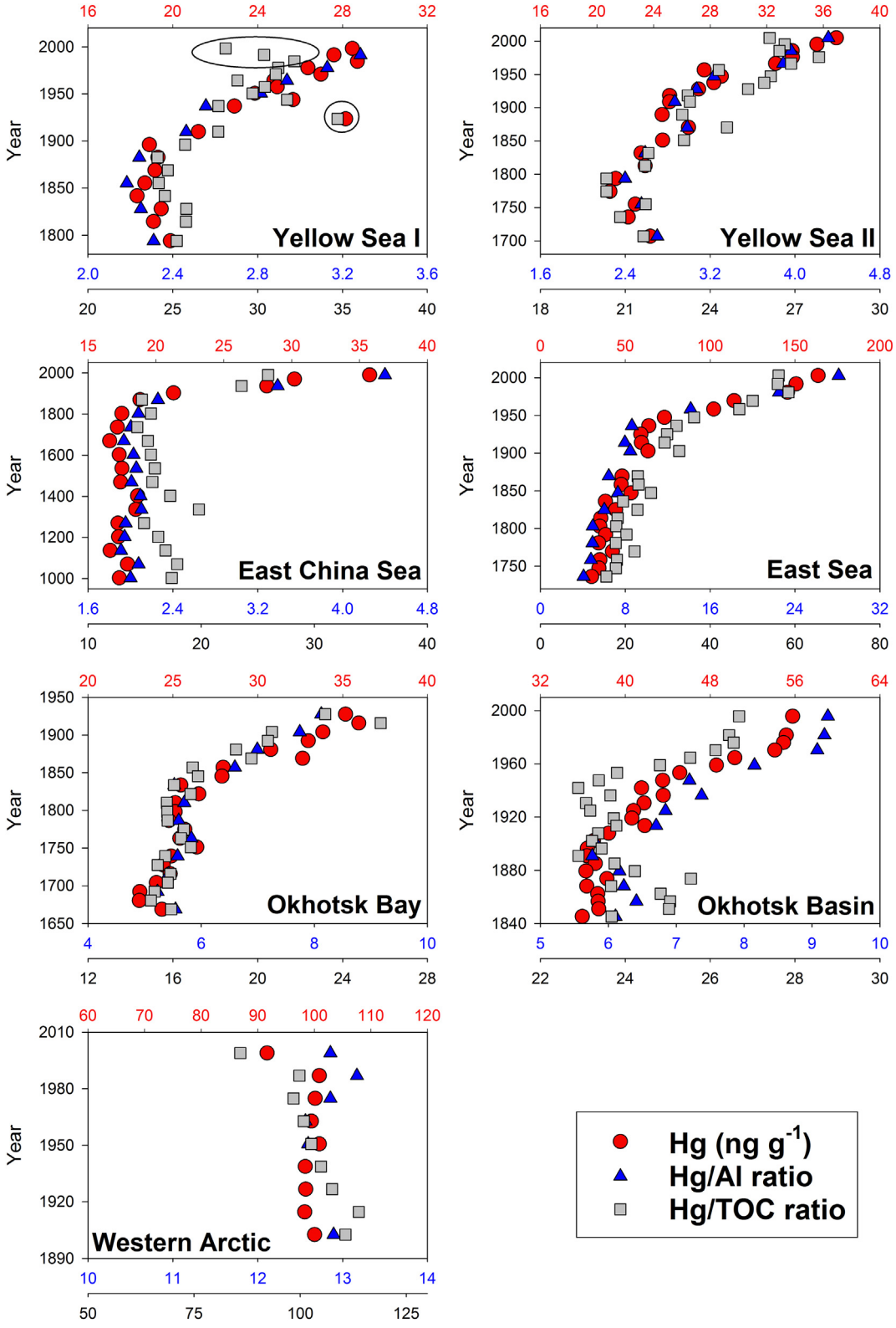


**Fig. 4.** The relationships between total Hg contents with Hg to Al or TOC ratios. The Hg contents (ng $g^{-1}$; red dot) and Hg to Al (blue triangle) or TOC (gray square) ratios in the core profiles from the Yellow ($n = 43$), East China ($n = 18$), East ($n = 23$) and Okhotsk ($n = 49$) Seas and western Arctic Ocean ($n = 9$). Circles in the Yellow Sea I were outliers. (For interpretation of the references to color in this figure legend, the reader is referred to the web version of this article.)

with the recent finding that the Arctic Hg is mainly derived from river discharge rather than atmospheric Hg deposition (Emmerton et al., 2013; Zhang et al., 2015). For example, the Hg input from the Yukon River was estimated to be 4.4 Mg $yr^{-1}$ (Schuster et al., 2011) that is insignificant compared to the input (581 Mg $yr^{-1}$) to the East China and Yellow Seas. Thus, the recent increase in the Hg content of Arctic sediments was largely confined to coastal areas that have received Hg derived from adjacent rivers, and is probably not from the atmospheric transport and deposition (Schuster et al., 2011; Emmerton et al., 2013; Zhang et al., 2015). In addition, the wet deposition of Hg over the Arctic

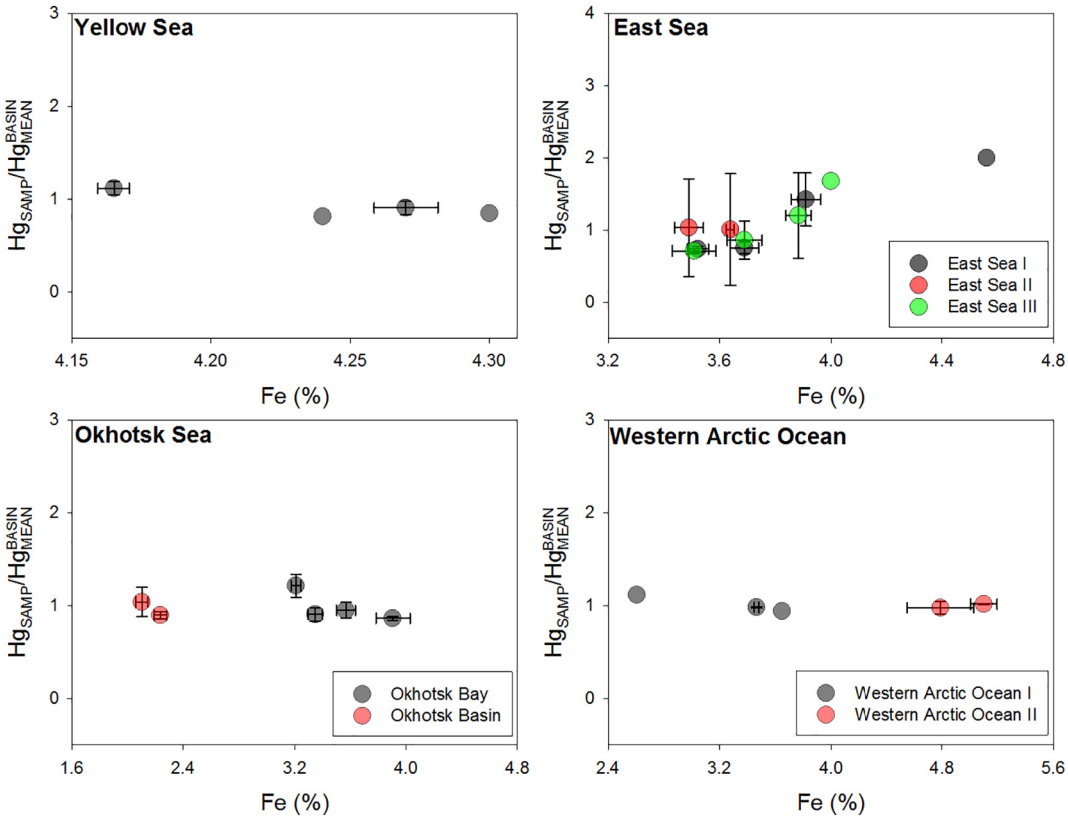


**Fig. 5.** The relationship between Fe (%) and $Hg_{SAMP}/Hg_{MEAN}^{BASIN}$ concentrations in the cores. These cores came from the Yellow, East and Okhotsk Seas and western Arctic Ocean. In order to minimize the effect of basin-to-basin difference, Hg contents ($Hg_{SAMP}$) were normalized to the corresponding basin-mean background Hg ($Hg_{MEAN}^{BASIN}$). (For interpretation of the references to color in this figure legend, the reader is referred to the web version of this article.)

Ocean was reported to be considerably lower (0.5–2.0 μg $m^{-2}$ $yr^{-1}$) (Kirk et al., 2012) than over the East China and Yellow Seas (24.8 μg $m^{-2}$ $yr^{-1}$) (Fu et al., 2016), confirming that the western Arctic Ocean has been far less affected by atmospheric $Hg^{ANTH}$.

It is noteworthy that $Hg^{ANTH}$ fluxes (5–14 μg $m^{-2}$ $yr^{-1}$) to selected locations (5 samples) in the Okhotsk Sea were abnormally high, suggesting that submarine hydrothermal activity may be a source of sediment Hg in these locations. In the vicinity of hydrothermal vents seawater $Hg^{2+}$ forms HgS (cinnabar) or is scavenged by metal hydroxides (oxidized Fe and Mn), and becomes incorporated into sediments. Therefore, the sediments enriched in Fe, Mn, and $S^o$ are generally found in the vicinity of the hydrothermal vents or submarine volcanoes (Boström and Fisher, 1969; Cox and McMurtry, 1981; Salinas-de-León et al., 2018). In the Okhotsk Sea the hydrothermal vents or submarine volcanoes near our sampling sites probably biased the surface $Hg^{ANTH}$ flux estimation, because the ferromanganese crust and brown color of sediments in these locations are signs of materials resulting from volcanic or hydrothermal activity (oxidized Fe and Mn enrichment) (Jin et al., 2011; Mikhailik et al., 2012; Salinas-de-León et al., 2018). However, this natural addition of Hg did not occur in the East China and Yellow Seas, which had the highest $Hg^{ANTH}$ flux.

A recent study reported that enhanced primary productivity could increase the sequestration of Hg by diatoms, eventually adding more Hg to the Southern Ocean sediments (Zaferani et al., 2018). However, our method using Eq. (3) (i.e. Hg content normalized by Al content) should reasonably account for differences in Hg content arising from differences in biological production among our study areas.

Finally, it is important to note that the recent increase in anthropogenic nitrate in the East China and Yellow Seas (Kim et al., 2011; Kim et al., 2014b) may result in a comparable increase in biological production, although a direct association between anthropogenic nitrate input and phytoplankton biomass is yet to be confirmed (Kim et al., 2014c). If such an association were to exist, the resulting increase in biological production would be expected also to increase the input of Hg into the sedimentary environment of the East China and Yellow Seas.

### 4.3. Down-core $Hg^{ANTH}$ flux in the Northwest Pacific Ocean

Historically, $Hg^{ANTH}$ emissions from the North America and Europe derived from silver mining, which reached peak activity in the 1880s. In recent times, Hg emissions have decreased in these countries because of the strict enforcement of legal regulations. However, $Hg^{ANTH}$ emissions in northeast Asian countries have continuously increased since 1900, with coal combustion and artisanal gold mining being two main sources (Street et al., 2011). Consistent with this, an increasing trend of $Hg^{ANTH}$ flux was observed in down-core sediments accumulated since 1900s in the East China, Yellow and East Seas, which largely reflects historical $Hg^{ANTH}$ emissions from China, Korea and Japan.

One interesting deviation from this general trend in $Hg^{ANTH}$ flux was observed in the Okhotsk basin, where a sharp increase was observed before 1960, followed by a plateau in the mid-1990s. This deviation appeared to be associated with Hg emissions from countries in the former Soviet Union. High levels of industrial activity in the former Soviet Union between 1920 and 1960 resulted in greater fossil fuel consumption, which in turn led to greater Hg emissions, whereas the economic crisis in that region after 1980 resulted in a dramatic decrease in fossil fuel consumption and hence to lower $Hg^{ANTH}$ emissions (Street et al., 2011; Maddison, 2006).

To confirm the recent increase in the accumulation of $Hg^{ANTH}$ in sediments in the East China, Yellow and East Seas, natural factors that could bias estimates of the sediment $Hg^{ANTH}$ content need to be properly accounted for. These include post-depositional digenesis, grain size (sediment texture), organic matter content, sedimentation rate, and methylation, all of which could affect the sediment Hg concentration

by mobilizing and redistributing Hg within the sediment cores (Fitzgerald et al., 2007).

Variations in grain size and organic matter content could also cause depth-core variations in Hg content, because these two factors strongly affect the Hg adsorption to sediments. This possibility was investigated by normalizing the Hg concentration to the concentrations of Al or TOC, because this normalization method can account for the effects of grain size and organic matter on Hg concentrations (Windom et al., 1989). The results showed that the depth profiles for Hg normalized to Al (Hg/Al) or TOC (Hg/TOC) were almost identical to the depth profile for Hg concentration. This congruence indicates that the effects of grain size and organic matter on the $Hg^{ANTH}$ flux profile were not significant, so did not affect our conclusions (Fig. 4). Note that for the Yellow Sea sediment core I, the deviations in the Hg/TOC ratio found in near-surface sediments and in the sediment dated to 1920 were probably caused by sampling error or bioturbation. Despite these deviations, the increasing trend of the Hg/TOC for the two sediment cores collected from the Yellow Sea was largely consistent.

The diagenesis of Fe and Mn redox cycling followed by the desorption of Hg onto oxides and hydroxides (Fe/Mn) can redistribute Hg vertically in sediment cores (Gobeil et al., 1999). However, we found no positive relationship between the concentrations of Hg and Fe in any sediment cores sampled from the Yellow and Okhotsk Seas or the western Arctic Ocean, indicating that sediment digenesis had little effect on the Hg profiles in cores taken from our study area (Fig. 5). A slight positive relationship in sediment cores sampled from the East Sea may be a sign of Fe reduction. However, the good agreement between the profiles of Hg content and those of Hg/Fe ratio confirmed little impact of Fe reduction on sediment Hg content (Fig. S4 in the Supplementary Information).

In addition, no change in sedimentation rate for the past 100 years (covering the upper 9–19 cm in sediment cores) (Fig. S5 in the Supplementary Information) indicates that sedimentation rate change as an explanation for any increase in the $Hg^{ANTH}$ flux is excluded. The high $Hg^{ANTH}$ flux observed in the East China, Yellow, and East Seas could also be because of sedimentary methylation in those basins. However, the concentration of MeHg accounts for <1% of the total Hg contents and demethylation is also simultaneously occurring (Gworek et al., 2016). Therefore, methylation was not a major factor dictating the $Hg^{ANTH}$ flux in the marine sediments of the basins investigated.

## 5. Conclusion

This study revealed a consistent signal of $Hg^{ANTH}$ deposition to sedimentary environments in the northwestern Pacific Ocean downwind of the Asian continent, through the formation of organo mercury complexes. The recent increase in $Hg^{ANTH}$ flux determined from several sediment core profiles provides compelling evidence of historical $Hg^{ANTH}$ input into open ocean sedimentary environments downwind of this industrialized continent.

## Acknowledgement

We thank to three anonymous referees for their critical comments. This work was primarily supported by the National Fisheries Research and Development Institute (R2018048) and by Mid-career Researcher Program (No. 2018R1A2A1A19019281) of the National Research Foundation of Korea (NRF). Partial supports were provided by Global Research Laboratory Program (No. 2013K1A1A2A02078278) of NRF, by "Iedo Ocean Research Station" project of Korea Hydrographic and Oceanographic Agency, by "Management of Marine Organisms causing Ecological Disturbance and Harmful Effects" funded by the Ministry of Oceans and Fisheries (MOF), by the NRF (2015M1A5A1037243, PN18090) and by National Marine Biodiversity Institute Research Program (2018M00500).

## Conflict of interest

The authors declare that they have no conflict of interest.

## Author contributions

H.K. and K.L. designed the study and wrote the manuscript. The analysis of data was performed by H.K., D.I.L., J.K. and S.I·N, collected samples and S.H., E.L., I.H., Y.J. and Y.Z. contributed to the manuscript with discussions and comments.

## Appendix A. Supplementary data

Supplementary data to this article can be found online at https://doi.org/10.1016/j.scitotenv.2018.11.076.

## References

Amos, H.M., Jacob, D.J., Kocman, D., Horowitz, H.M., Zhang, Y., Dutkiewicz, S., Horvat, M., Corbitt, E.S., Krabbenhoft, D.P., Sunderland, E.M., 2014. Global biogeochemical implications of mercury discharges from rivers and sediment burial. Environ. Sci. Technol. 48, 9514–9522.

Astakhov, A.S., Gorbarenko, S.A., Bakhareva, G.A., Gretskaya, E.V., Sattarova, V.V., 2005. Distribution and accumulation rate of ore elements in Holocene and Late Glacial Sediments of the Deryugin Basin, Sea of Okhotsk. Lithol. Miner. Resour. 45, 47–61.

Blum, J.D., Sherman, L.S., Johnson, M.W., 2014. Mercury isotopes in earth and environmental sciences. Annu. Rev. Earth Planet. Sci. 42 (1), 249–269.

Boström, K., Fisher, D.E., 1969. Distribution of mercury in East Pacific sediments. Geochim. Cosmochim. Ac. 33, 743–745.

Chakraborty, P., Sarkar, A., Vudamala, K., Naik, R., Nath, B.N., 2015. Organic matter—a key factor in controlling mercury distribution in estuarine sediment. Mar. Chem. 173 (2), 302–309.

Chen, C., Zheng, B., Jiang, X., Zhao, Z., Zhan, Y., Yi, F., Ren, J., 2013. Spatial distribution and pollution assessment of mercury in sediments of Lake Taihu, China. J. Environ. Sci. 25, 316–325.

Chen, M., Kim, J.-H., Nam, S.-I., Niessen, F., Hong, W.-L., Kang, M.-H., Hur, J., 2016. Production of fluorescent dissolved organic matter in Arctic Ocean sediments. Sci. Rep. 6, 39213.

Corbitt, E.S., Jacob, D.J., Holmes, C.D., Streets, D.G., Sunderland, E.M., 2011. Global source–receptor relationships for mercury deposition under present-day and 2050 emissions scenarios. Environ. Sci. Technol. 45, 10477–10484.

Covelli, S., Faganeli, J., Horvat, M., Brambati, A., 2001. Mercury contamination of coastal sediments as the result of long-term cinnabar mining activity (Gulf of Trieste, northern Adriatic sea). Appl. Geochem. 16, 541–558.

Cox, M.E., McMurtry, G.M., 1981. Vertical distribution of mercury in sediments from the East Pacific rise. Nature 289, 789–792.

Daskalakis, K.D., O'Connor, T.P., 1995. Normalization and elemental sediment contamination in the coastal United States. Environ. Sci. Technol. 29 (2), 470–477.

Deng, B., Zhang, J., Wu, Y., 2006. Recent sediment accumulation and carbon burial in the East China Sea. Glob. Biogeochem. Cycles 20, GB3014.

Dou, Y., Yang, S., Lim, D.-I., Jung, H.-S., 2015. Provenance discrimination of last deglacial and Holocene sediments in the southwest of Cheju Island, East China Sea. Palaeogeogr. Palaeoclimatol. Palaeoecol. 422, 25–35.

Emmerton, C.A., Graydon, J.A., Gareis, J.A.L., St. Louis, V.L., Lesack, L.F.W., Banack, J.K.A., Hicks, F., Nafziger, J., 2013. Mercury export to the Arctic Ocean from the Machenzie River. Canada. Environ. Sci. Technol. 47 (14), 7644–7654.

Engstrom, D.R., 2007. Fish respond when the mercury rises. Proc. Natl. Acad. Sci. U. S. A. 104, 16394–16395.

Enrico, M., Le Roux, G., Heimbürger, L.E., Van Beek, P., Souhaut, M., Chmeleff, J., Sonke, J.E., 2017. Holocene atmospheric mercury levels reconstructed from peat bog mercury stable isotopes. Environ. Sci. Technol. 51, 5899–5906.

Fang, T.-H., Li, J.-Y., Feng, H.-M., Chen, H.-Y., 2009. Distribution and contamination of trace metals in surface sediments of the East China Sea. Mar. Environ. Res. 68, 178–187.

Fitzgerald, W.F., Engstrom, D.R., Lamborg, C.H., Tseng, C.-M., Balcom, P.H., Hammerschmidt, C.R., 2005. Modern and historic atmospheric mercury fluxes in northern Alaska: global sources and Arctic depletion. Environ. Sci. Technol. 39, 557–568.

Fitzgerald, W.F., Lamborg, C.H., Hammerschmidt, C.R., 2007. Marine biogeochemical cycling of mercury. Chem. Rev. 107, 641–662.

Fu, X., Yang, X., Lang, X., Zhou, J., Zhang, H., Yu, B., Yan, H., Lin, C.-J., Feng, X., 2016. Atmospheric wet and litterfall mercury deposition at urban and rural sites in China. Atmos. Chem. Phys. 16, 11547–11562.

Gobeil, C., Macdonald, R.W., Smith, J.N., 1999. Mercury profiles in sediments of the Arctic Ocean Basins. Environ. Sci. Technol. 33, 4194–4198.

Gworek, B., Bemowska-Kałabun, O., Kijeńska, M., Wrzosek-Jakubowska, J., 2016. Mercury in marine and oceanic waters: a review. Water Air Soil Pollut. 227, 371.

Hermanns, Y.-M., Biester, H., 2013. Anthropogenic mercury signals in lake sediments from southernmost Patagonia, Chile. Sci. Total Environ. 445–446, 126–135.

Holmes, C.D., Jacob, D.J., Corbitt, E.S., Mao, J., Yang, X., Talbot, R., Slemr, F., 2010. Global atmospheric model for mercury including oxidation by bromine atoms. Atmos. Chem. Phys. 10, 12037–12057.

Hong, G.H., Kim, S.H., Chung, C.S., Kang, D.-J., Shin, D.-H., Lee, H.J., Han, S.-J., 1997. $^{210}$Pb-derived sediment accumulation rates in the southwestern East Sea (Sea of Japan). Geo-Mar. Lett. 17, 126–132.
Hu, L., Shi, X., Bai, Y., Qiao, S., Li, L., Yu, Y., Yang, G., Ma, D., Guo, Z., 2016. Recent organic carbon sequestration in the shelf sediments of the Bohai Sea and Yellow Sea, China. J. Mar. Syst. 155, 50–58.
Huang, S.S., Fan, D.F., Chen, B., Jin, Y., 2005. A temporal assessment on ecological risk caused by heavy metals in north Taihu basin. Jiangsu Geo. 29, 43–45.
Iricanin, N., Trefry, H.H., 1990. Trace Metal Distribution in Sediments from the Bering Sea. U.S. Fish Wildlife Service Biology Report.
Jin, Y.K., Kim, Y.-G., Baranov, B., Shoji, H., Obzhirov, A., 2011. Distribution and expression of gas seeps in a gas hydrate province of the northeastern Sakhalin continental slope, Sea of Okhotsk. Mar. Pet. Geol. 28, 1844–1855.
Johannessen, S.C., Macdonald, R.W., Eek, K.M., 2005. Historical trends in mercury sedimentation and mixing in the Strait of Georgia, Canada. Environ. Sci. Technol. 39, 4361–4368.
Kim, T.-W., Lee, K., Najjar, R.G., Jeong, H.-D., Jeong, H.J., 2011. Increasing N abundance in the norhwestern Pacific Ocean due to atmospheric nitrogen deposition. Science 334, 505–509.
Kim, I.-N., Lee, K., Gruber, N., Kail, D.M., Bullister, J.L., Yang, S., Kim, T.-W., 2014b. Increasing anthropogenic nitrogen in the North Pacific Ocean. Science 346, 1102–1106.
Kim, T.-W., Lee, K., Duce, R., Liss, P., 2014c. Impact of atmospheric nitrogen deposition on phytoplankton productivity in the South China Sea. Geophys. Res. Lett. 41, 3156–3162.
Kim, H., Lee, K., Lim, D.-I., Nam, S.-I., Kim, T.-W., Yang, J.-Y., Ko, Y.H., Shin, K.H., Lee, E., 2017. Widespread anthropogenic nitrogen in northwestern Pacific Ocean sediments. Environ. Sci. Technol. 51 (11), 6044–6052.
Kim, J., Lim, D., Jung, D., Kang, J., Jung, H., Woo, H., Jeong, K., Xu, Z., 2018. Sedimentary mercury (Hg) in the marginal seas adjacent to Chinese high-Hg emissions: source-to-sink, mass inventory, and accumulation history. Mar. Pollut. Bull. 128, 428–437.
Kirk, J.L., Lehnherr, I., Andersson, M., Braune, B.M., Chan, L., Dastoor, A.P., Durnford, D., Gleason, A.L., Loseto, L.L., Steffen, A., Louis, St., L, V., 2012. Mercury in Arctic marine ecosystems: sources, pathways and exposure. Environ. Res. 119, 64–87.
Lepak, R.F., Yin, R., Krabbenhoft, D.P., Ogorek, J.M., DeWild, J.F., Holsen, T.M., Hurley, J.P., 2015. Use of stable isotope signatures to determine mercury sources in the Great Lakes. Environ. Sci. Technol. Lett. 2, 335–341.
Lim, D.I., Choi, J.Y., Jung, H.S., Rho, K.C., Ahn, K.S., 2007. Recent sediment accumulation and origin of shelf mud deposits in the Yellow and East China Seas. Prog. Oceanogr. 73, 145–159.
Lim, D.-I., Jung, H.S., Kim, K.T., Shin, H.H., Jung, S.W., 2012. Sedimentary records of metal contamination and eutrophication in Jinhae-Masan Bay, Korea. Mar. Pollut. Bull. 64, 2542–2548.
Lim, D., Kim, J., Xu, Z., Jeong, K., Jung, H., 2017. New evidence for Kuroshio inflow and deepwater circulation in the Okinawa Trough, East China Sea: sedimentary mercury variations over the last 20 kyr. Paleoceanography 32, 571–579.
Liu, M., Chen, L., Wang, X., Zhang, W., Tong, Y., Ou, L., Xie, H., Shen, H., Ye, X., Deng, C., Wang, H., 2016. Mercury export from Mainland China to adjacent seas and its influence on the marine mercury balance. Environ. Sci. Technol. 50, 6224–6232.
Loring, D.H., Rantala, R.T.T., 1992. Manual for the geochemical analyses of marine sediments and suspended particulate matter. Earth Sci. Rev. 32, 235–283.
Maddison, A., 2006. The World Economy. Paris, France: Development Centre of the Organisation for Economic Co-operation and Development. OECD, pp. 400–600.
Mikhailik, P.E., Khanchuk, A.I., Mikhailik, E.V., Ivanov, M.V., Elovskii, E.V., Mel'nikov, M.E., 2012. New data on the concentration of mercury in ferromanganese crusts from submarine seamounts of the Northwest Pacific. Dokl. Earth Sci. 447, 1327–1332.
Morris, M.A., Spencer, K.L., Belyea, L.R., Branfireun, B.A., 2014. Temporal and spatial distributions of sediment mercury in restored coastal saltmarshes. Mar. Chem. 167, 150–159.
Müller, R.D., Qin, X., Sandwell, D.T., Ditkiewicz, A., Willams, S.E., Flament, N., Maus, S., Seton, M., 2016. The GPlates portal: cloud-based interactive 3D visualization of global geophysical and geological data in a web browser. PLoS One 11 (3), e0150883.
Nelson, D.W.S., 1996. Part 3. Chemical Methods. In: Sparks, D.R. (Ed.), Methods of Soil Analysis. Soil Sci. Soc. Am., Madison.
Oguri, K., Harada, N., Tadai, O., 2012. Excess $^{210}$Pb and $^{137}$Cs concentrations, mass accumulation rates, and sedimentary processes on the Bering Sea continental shelf. Deep-Sea Res. Pt. II 61–64, 193–204.
Percival, L.M.E., Witt, M.L.I., Mather, T.A., Hermoso, M., Jenkyns, H.C., Hesselbo, S.P., Suwaidi, A.H., Storm, M.S., Xu, W., Ruhl, M., 2015. Globally enhanced mercury deposition during the end-Pliensbachian extinction and Toarcian OAE: a link to the Karoo–Ferrar Large Igneous Province. Earth Planet Sc. Lett. 428, 267–280.
Salinas-de-León, P., Phillips, B., Ebert, D., Shivji, M., Cerutti-Pereyra, F., Ruck, C., Fisher, C.R., Marsh, L., 2018. Deep-sea hydrothermal vents as natural egg-case incubators at ghe Galapagos Rift. Sci. Rep. 8 (1), 1788.
Schuster, P.F., Schuster, P.F., Krabbenhoft, D.P., Naftz, D.L., Cecil, L.D., Olson, M.L., Dewild, J.F., Susong, D.D., Green, J.R., Abbott, M.L., 2002. Atmospheric mercury deposition during the last 270 years: a glacial ice core record of natural and anthropogenic sources. Environ. Sci. Technol. 36 (11), 2303–2310.
Schuster, P.F., Striegl, R.G., Aiken, G.R., Krabbenhoft, D.P., Dewild, J.F., Butler, K., Kamark, B., Dornblaster, M., 2011. Mercury export from the Yukon river basin and potential response to a changing climate. Environ. Sci. Technol. 45 (21), 9262–9267.
Sherman, L.S., Blum, J.D., Keeler, G.J., Demers, J.D., Dvonch, J.T., 2012. Investigation of local mercury deposition from a coal-fired power plant using mercury isotopes. Environ. Sci. Technol. 46, 382–390.
Song, K.-H., Choi, K.-Y., Kim, C.-J., Kim, Y.-I., Chung, C.-S., 2015. Assessment of the governance system for the management of the East Sea-Jung dumping site, Korea through analysis of heavy metal concentrations in bottom sediments. Ocean Sci. J. 50, 721–740.
Street, D.G., Devane, M.K., Lu, Zifeng, Bond, T.C., Sunderland, E.M., Jacob, D.J., 2011. All-time releases of mercury to the atmosphere from human activities. Environ. Sci. Technol. 45 (24), 10485–10491.
Sun, R., Sonke, J.E., Heimbürger, L.-E., Belkin, H.E., Liu, G., Shome, D., Cukrowska, E., Liousse, C., Pokrovsky, O.S., Streets, D.G., 2014. Mercury stable isotope signatures of world coal deposits and historical coal combustion emissions. Environ. Sci. Technol. 48, 7660–7668.
Sunderland, E.M., Mason, R.P., 2007. Human impacts on open ocean mercury concentrations. Glob. Biogeochem. Cycles 21, GB4022.
Wiederhold, J.G., Skyllberg, U., Drott, A., Jiskra, M., Jonsson, S., Björn, E., Bourdon, B., Kretzschmar, R., 2015. Mercury isotope signatures in contaminated sediments as a tracer for local industrial pollution sources. Environ. Sci. Technol. 49, 177–185.
Windom, H.L., Schropp, S.J., Calder, F.D., Ryan, J.D., Smith, R.G., Burney, L.C., Lewis, F.G., Rawlinson, C.H., 1989. Natural trace metal concentrations in estuarine and coastal marine sediments of the southeastern United States. Environ. Sci. Technol. 23, 314–320.
Yin, R., Feng, X., Chen, B., Zhang, J., Wang, W., Li, X., 2015. Identifying the sources and processes of mercury in subtropical estuarine and ocean sediments using hg isotopic composition. Environ. Sci. Technol. 49, 1347–1355.
Zaferani, S., Marta, P.-R., Harald, B., 2018. Diatom ooze—a large marine mercury sink. Science 361, 797–800.
Zhang, Y., Jacob, D.J., Dutkiewicz, S., Amos, H.M., Long, M.S., Sunderland, E.M., 2015. Biogeochemical drivers of the fate of riverine mercury discharged to the global and Arctic oceans. Glob. Biogeochem. Cycles 29, 854–864.
Zhang, Y., Jacob, D.J., Horowitz, H.M., Amos, H.M., Krabbenhoft, D.P., Slemr, F., St. Louis, V.L., Sunderland, E.M., 2016. Observed decrease in atmospheric mercury explain by global decline in anthropogenic emissions. Proc. Natl. Acad. Sci. U. S. A. 113, 526–531.
Zhou, G., Sun, B., Zeng, D., Wei, H., Liu, Z., Zhang, B., 2014. Vertical distribution of trace elements in the sediment cores from major rivers in East China and its implication on geochemical background and anthropogenic effects. J. Geochem. Explor. 139, 53–67.
Zohar, I., Bookman, R., Levin, N., de Stigter, H., Teutsch, N., 2014. Contamination history of lead and other trace metals reconstructed from an urban winter pond in the eastern Mediterranean Coast (Israel). Environ. Sci. Technol. 48, 13592–13600.